Original Paper

Numerical Investigative Modeling of Changes Within the Patuha Geothermal Reservoir and Its Production Sustainability Under Two Different Conversion Technologies

Heru Berian Pratama [1,2,4] Sutopo,[1,2] Jonathan Sharon Widiatmo,[1] and Ali Ashat[1,3]

An integrated numerical modeling of reservoir and power plant thermodynamics is proposed to assess the Patuha geothermal field development strategy. Power plant technologies, namely as dry-steam cycle unit (DSCU) and integrated geothermal combined-cycle unit (IGCCU), were selected for field development strategy options. TOUGH2 was used to simulate the effects of these technologies on reservoir production sustainability. The selection of power plant technology and field production strategy clearly affects the performance of the reservoir. The simulation results show that the IGCCU is less sustainable if hot fluid is produced only from the steam zone. However, the energy extraction from the brine zone is proven advantageous to maintain the steam zone pressure. In addition, higher injection rates into the brine zone from IGCCU power plant can yield to higher electrical power generation than DSCU.

INTRODUCTION

The Patuha geothermal field is located in Bandung and Cianjur Districts, West Java Province, Indonesia. The field is operated by PT Geo Dipa Energi (GDE) and it has been generating 55 MW of electricity since 2014. Raharjo et al. (2016) said that Patuha is a volcano-hosted vapor geothermal systems along with Karaha Talaga-Bodas (Nemčok et al. 2007; Prabata et al. 2019; Sutopo et al. 2019), Wayang Windu (Bogie et al. 2008), Kamojang (Suryadarma et al. 2010) and Darajat (Intani et al. 2020) in West Java, Indonesia. However, Layman and Soemarinda (2003) and Elfina (2017) stated that Patuha is divided into two zones with a 220–260 °C productive reservoir. The Patuha Geothermal System consists of three reservoirs associated with the area of Kawah Putih, Kawah Ciwidey, and Kawah Cibuni (Ashat et al. 2019a). The Patuha is a vapor-dominated reservoir with a steam zone above the deep liquid reservoir. Therefore, it is a unique type of reservoir since both reservoirs (steam and liquid) exist simultaneously. Most of the production wells are in the steam zone, but several wells also hit the liquid zone. The fact that is steam zone and brine reservoirs exist simultaneously raised a question on what type of power plant should be used to optimize resource sustainability.

[1] Geothermal Engineering Master's Program, Faculty of Mining and Petroleum Engineering, Institut Teknologi Bandung, Jl. Ganesha 10, Bandung 40132, Indonesia.
[2] Geothermal Engineering Research Group, Faculty of Mining and Petroleum Engineering, Institut Teknologi Bandung, Jl. Ganesha 10, Bandung 40132, Indonesia.
[3] Department of Earth Resources Engineering, Faculty of Engineering, Kyushu University, Fukuoka 819-0395, Japan.
[4] To whom correspondence should be addressed; e-mail: heru.berian@geothermal.itb.ac.id

There are three primary power plant types: dry steam, flash steam, and binary (DiPippo 2012, 2015a). Dry-steam power plant is commonly used in steam-dominated or dry-steam reservoirs, i.e., the Geysers (Sanyal 2000), Darajat (Alamsyah et al. 2005; Hoang et al. 2005), Kamojang (Suryadarma et al. 2010), Larderello (Romagnoli et al. 2010), while flash steam power plants are found in liquid-dominated reservoirs, i.e., Wairakei (Bixley et al. 2009), Lahendong (Koestono et al. 2010), Wayang Windu (Mulyadi and Ashat 2011). For a fully liquid phase reservoir, binary power plant is commonly used. The Patuha reservoir, on the other hand, differs from a two-phase reservoir since the top part is steam dominated, while the bottom part is fully occupied by hot liquid water (Ashat and Pratama 2018; Ashat et al. 2019a, b). The existing 55 MW Patuha power plant utilizes the dry-steam cycle to extract energy only from the steam zone.

The Patuha geothermal field has unique reservoir characteristics; therefore, it has an opportunity to utilize the deep liquid reservoir using a binary cycle. Taking into consideration the thermodynamic efficiency and the geothermal fluid characteristics, an integrated geothermal combined-cycle unit (IG-CCU) was selected as an alternative development for the energy conversion cycle in Patuha. In Indonesia, this type of power plant has been used in Sarulla since 2017 (Wolf and Gabbay 2015).

The technical feasibility and sustainability of geothermal power plants do not only deal with technical optimization but also with how to match characteristics and capacity of the reservoir to the power plant. From this point of view, the first and most important activity is a proper investigation of the behavior and performance of the geothermal reservoir considering different ways of operation and exploitation scenarios. It can be obtained with numerical analysis. Therefore, reservoir modeling is a powerful tool available for this purpose.

Geothermal resource assessment is an essential aspect of field development. State-of-the-art research in resource assessment is the use of probabilistic method, i.e., experimental design (ED) and response surface method (RSM) with a numerical model. ED and RSM allow the integration of reservoir numerical model and uncertainty analysis (Quinao and Zarrouk 2018; Ashat and Pratama 2018; Ashat et al. 2019b; Prabata et al. 2019; Supijo et al. 2019; Sutopo et al. 2019; Pratama et al. 2020; Supijo et al. 2020). Numerical modeling of geothermal fields can be useful for predicting reservoir performances by various production-injection strategies, considering different exploitation scenarios in order to predict the sustainability of reservoir in the future and to analyze the effects of reinjection and required number of make-up wells to maintain the specified fluid production. Vapor-dominated reservoirs require an appropriate reinjection strategy. Kaya et al. (2011) and Rivera Diaz et al. (2016) stated that it is beneficial to inject the water directly above the depleted reservoir and close to the production wells.

The calculation of a geothermal field capacity based on numerical modeling has been widely used. The method has been applied in several fields such as Wairakei (Mannington et al. 2004; O'Sullivan et al. 2009), Momotombo (Porras et al. 2007; Franco and Vaccaro 2012), Kamojang (Suryadarma et al. 2010), Larderello (Romagnoli et al. 2010), Hatchobaru (Yahara and Tokita 2010), Ahuachapan (Monterrosa and Montalvo López 2010), Sabalan (Noorollahi and Itoi 2011) and Karaha Talaga-Bodas (Sutopo et al. 2019). Numerical reservoir modeling is the most powerful tool available to investigate sustainable management of geothermal resources. Previous studies (Romagnoli et al. 2010; Supijo et al. 2018; Ashat et al. 2019a; Lesmana et al. 2019; Seyedrahimi-Niaraq et al. 2019; Hamdani et al. 2020) state that numerical reservoir modeling is an essential step in geothermal exploration to accomplish more accurate conceptual models and define exploration strategies. Therefore, geosciences, reservoir & production engineering, and thermal engineering are integrated aspects in the sustainable design of geothermal plants. The behavior of a geothermal reservoir has to be estimated before the design of the plant (technologies, operating conditions). Thus, a reliable strategy for the future development of geothermal power production for sustainability should integrate the "Reservoir-Plant" approach. Numerical reservoir modeling appears to be a fundamental instrument for a synthetic and operative design of geothermal power plants. For this reason, a multidisciplinary approach is necessary to solve the challenges in geothermal field exploitation that is sustainable reservoir production.

The integration of the numerical reservoir and power plant thermodynamic model is a fundamental instrument for a synthetic and operative for the Patuha geothermal field. This study aims to define which power plant cycle or combination of power plant cycles gives the best production sustainability for a specific generating capacity. Numerical reser-

voir modeling was used to simulate the effect of each power generating scenario on reservoir production sustainability. Each power generating scenario was modelled thermodynamically.

NUMERICAL RESERVOIR MODEL

The Patuha reservoir numerical model has been developed previously by Ashat and Pratama (2018). The numerical model in this study is limited to Kawah Ciwidey reservoir that generates 55 MW production from the steam cap. The numerical model rotated parallel with Kawah Ciwidey fault as the main fault. The numerical model (Table 1) has a grid size of 5.5×5.5 km with rectangular mesh (250×250 m). The model is divided into 15 layers corresponding to 3.01 km in total thickness (2010 masl to -1000 masl. The layers have different thickness depending on the region. The thickness of the atmosphere, reservoir, and bottom layer are 10
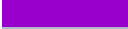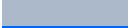
m, 200 m, and 500 m, respectively. The total blocks from the model is 7260 blocks. The top layer representing the atmospheric condition was set homogenously at 1 bar and 25 °C for initial pressure and temperature condition, respectively. The heat source at the bottom layer was set at 120 bar and 317 °C, which is based on the conceptual model with inflow around Mt. Patuha and Mt. Urug. The side boundary uses hydrostatic pressure and normal temperature gradient to represent the surrounding environment condition. The side boundary of the model is impermeable, with no flows of both heat and mass during natural state conditions.

The rock parameters are assigned to define a particular type of material properties such as specific heat, wet heat conductivity, rock density, porosity, and permeability (x, y, z-direction) in the TOUGH2 V.2.0 (Pruess et al. 1999). The most essential property in natural state calibration is permeability and porosity. The permeability will control the magnitude and the direction of mass and heat flow, and the distribution of pressure as well as temperature. The anisotropy of rock permeability was considered only for the ratio between vertical (k_z) and horizontal permeability (k_{xy}). The relative permeability uses Corey's Curve and has been assigned to all material rock data. This parameter has an impact on the mobility of liquid phase within the vapor-dominated reservoir under steady state conditions and during reservoir exploitation. Table 2 shows all the cali-

Table 1. Summary of the Patuha numerical model

Items	Value
Vertical layers	15 layers
Total thickness	3.01 km (2010 to − 1000 masl)
Area size	5.5 × 5.5 km
Grid type	Rectangular
Grid area size	250 × 250 m

Table 2. Material properties of the Patuha numerical model, the values of porosity and rock permeability based on the previous studies (Ashat and Pratama 2018; Ashat et al. 2019a, b)

Material	Color	Porosity	Horizontal permeability k_{xy} (m²)	Vertical permeability k_z (m²)
RESV1		0.10	1.00E−13	5.00E−14
RESV2		0.10	8.00E−14	4.00E−14
RESV3		0.10	8.00E−14	4.00E−14
RESL1		0.10	5.00E−14	2.00E−14
RESL2		0.07	4.00E−14	2.00E−14
RESL3		0.05	2.00E−14	1.00E−14
RSVG		0.08	2.00E−15	1.00E−15
FCIWI		0.15	3.00E−14	3.00E−14
FBDTL		0.125	2.50E−14	2.50E−14
FCIMA		0.125	2.00E−14	2.00E−14
FBLTG		0.10	3.00E−15	3.00E−15
SEAL1		0.05	8.00E−15	8.00E−15
UPZ05		0.10	8.00E−14	4.00E−14
UPZ02		0.10	8.00E−13	4.00E−13
SEAL2		0.05	1.00E−17	1.00E−17
HEATS		0.05	1.00E−14	1.00E−15

brated permeability and porosity data. Other material properties such as density, specific heat, and wet heat conductivity are 2500–2600 kg/m^3, 1000–1100 J/(kg °C), and 2 W/(m °C), respectively.

The location of each well on the numerical model is shown in Figure 1. The fault orientations divide the reservoir into four areas, as shown in Figure 2. Later, it becomes clear that the faults act
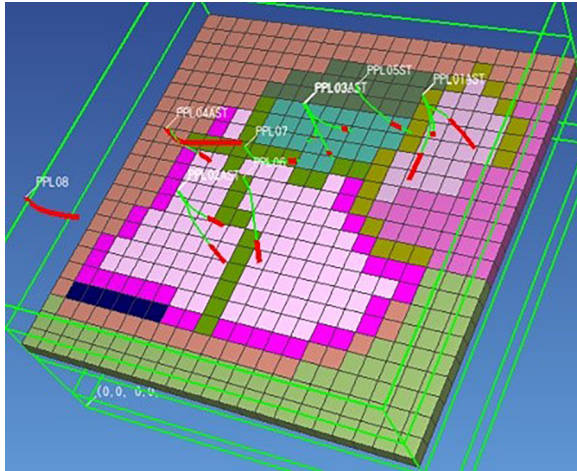
Fig. 1. Existing well locations (green and red line) in the numerical model. The colors of each grid block represent the material properties given in Table 2.
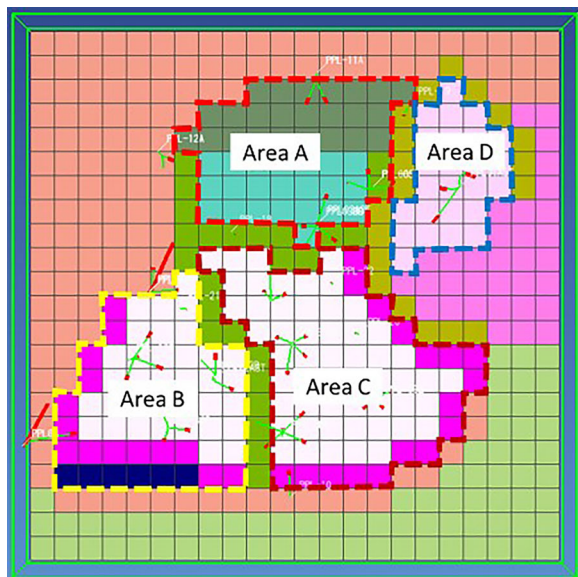
Figure 2. Top view of the reservoir numerical model at steam zone (900 masl) and four reservoir areas (**a**, **b**, **c**, and **d**) separated by fault orientation. The colors of each grid block represent the material properties given in Table 2.

more like a barrier between each area. This model has been calibrated using static well pressure and temperature data. The model has also been further recalibrated during production history matching using actual data of well production history. The results of natural state modeling and production history matching show a good match between simulation output and field data as the previous result (Ashat and Pratama 2018; Ashat et al. 2019a, b). Based on the results of the previous studies by Ashat et al. (2019b), the Kawah Ciwidey reservoir has a reserve of 128 MW.

POWER PLANT THERMODYNAMIC MODEL

The geothermal power plants have evolved from a simple system (dry-steam) for the vapor-dominated geothermal field to complicated multi-flash and hybrid system design to operate on liquid-dominated that represents a wide range of reservoir fluid temperatures. The performance of a geothermal power plant may be taken in several ways from the practical, specific geofluid consumption (SGC), which is geothermal fields-specific, to thermal efficiency, which applies strictly to binary cycle plants to utilization efficiency (DiPippo 2015b). A worldwide review (Zarrouk and Moon 2014) from 94 geothermal plants stated that conversion efficiencies as a function of the reservoir enthalpy are given for single flash/dry steam, double flash, binary plants, and for a generic geothermal power plant. The conversion efficiency of binary plants has the lowest certainty, mainly because of the frequent use of air cooling, which is profoundly affected by local and seasonal changes in ambient temperatures.

Dry-Steam Cycle Unit (DSCU)

The schematic diagram for a DSCU is shown in Figure 3. Dry-steam produced from production wells is supplied to the steam turbine and it exits the turbine from the turbine exhaust. Steam from turbine exhaust (vapor–liquid mixture) is then condensed in the condenser and flowed to the cooling tower to be cooled further. The Patuha power plant uses this similar process on the Unit-1, generating 55 MW with SGC of 2.016 kg/s/MW. The thermodynamic process of a such system could be represented in Figure 4 and the calculation based on
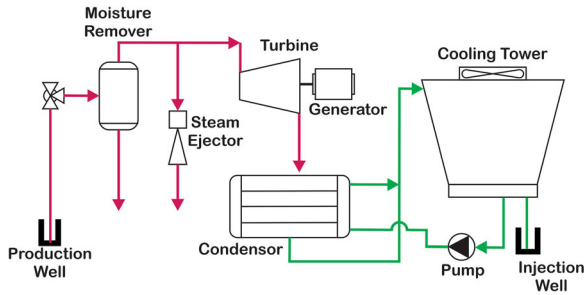
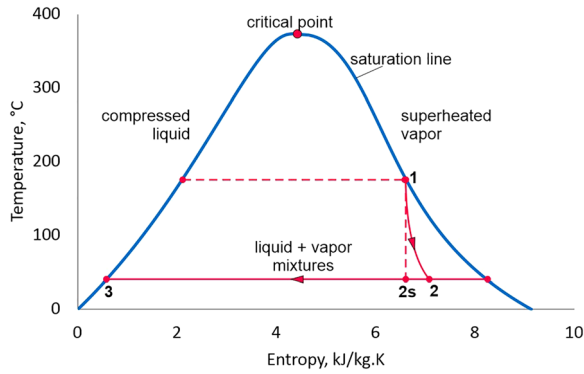**Figure 3.** Typical dry-steam cycle unit process flow.

Figure 4. Temperature–entropy diagram for a dry-steam plant in Patuha with saturated steam at the turbine inlet. The turbine expansion process 1–2, isentropic process 1–2 s, and the heat are rejected to the surroundings in the condenser via the cooling water in process 2–3.

DiPippo (2012, 2015a). In this process, the expansion of saturated steam (Process 1–2) releases energy harnessed by the turbine to generate electricity. The turbine expansion process generates slightly less power output than the ideal, isentropic process 1–2 s.

The mathematical formula for the dry-steam cycle thermodynamic model is shown in Eqs. (1)–(6). The goal of the power plant thermodynamic model is to find the value of SGC. The simulated steam production profile (in kg/s or ton/h) can be converted to MW by dividing it with SGC. Equation 6 requires a parameter in which value is specific to the turbine design (constant c). The value of constant c could be taken arbitrarily, but for this study, the value of c is obtained by back calculating the existing turbine parameter in the Patuha power plant.

$$w_t = h_1 - h_2 \qquad (1)$$

$$\eta_t = \frac{h_1 - h_2}{h_1 - h_{2s}} \qquad (2)$$

$$\dot{W}_t = \dot{m}_s w_t \qquad (3)$$

$$h_{2s} = h_3 + [h_g - h_3]\left[\frac{s_1 - s_3}{s_g - s_3}\right] \qquad (4)$$

$$h_2 = \frac{h_1 - A\left[1 - \frac{h_3}{h_g - h_3}\right]}{1 + \frac{A}{h_g - h_3}} \qquad (5)$$

$$A \equiv c(h_1 - h_{2s}) \qquad (6)$$

where w_t is the turbine specific energy (kJ/kg), $\dot{W}_t$ is the power (kJ/s or kW) generated by turbine, η_t is the turbine efficiency $\dot{m}_s$ steam mass flow rate (kg/s), A *is* turbine specific parameter A (kJ/kg), c is the turbine specific parameter, h_1, h_2, h_2s, h_g, h_3 are the specific enthalpy (kJ/kg) of fluid at different states, and s_1, s_3, s_g are entropy (kJ/kg K) of fluid at different states.

Integrated Geothermal Combined-Cycle Unit (IGCCU)

Figure 5 shows a typical IGCCU, which consists of three subunits: steam turbine generator (STG), ORC Bottoming, and ORC Brine. The process starts with geothermal fluid entering the separation system. The steam is then fed to the STG and goes through the condensing process in the ORC Bottoming sub-unit. The ORC Bottoming (Fig. 6) sub-unit extracts energy by condensing the steam to generate electricity. ORC Brine (Fig. 8) is similar to a common Organic Rankine Cycle Unit, which extracts heat energy from the brine to generate electricity and adds a recuperator to increase efficiency. One of the advantages of using a combined-cycle unit is that the steam specific consumption is more stable concerning noncondensable gas (NCG) content changes than the dry-steam cycle unit (Kaypakoglu and Barbon 2019). For the dry-steam cycle unit to operate efficiently at high NCG content, it requires another kind of NCG removal system other than a steam jet ejector. Some alternative solutions are using a compressor system or liquid ring vacuum pump (Ozcan and Gokcen 2013). On the other hand, IGCCU is prone to solid deposition (such as silica scaling) in its vaporizer unit. Some simple solutions
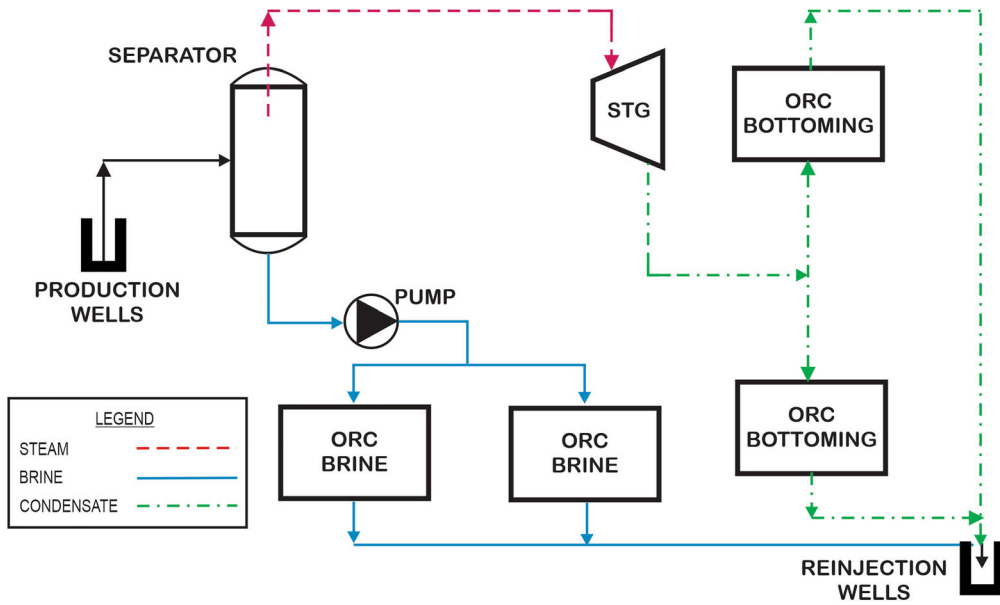
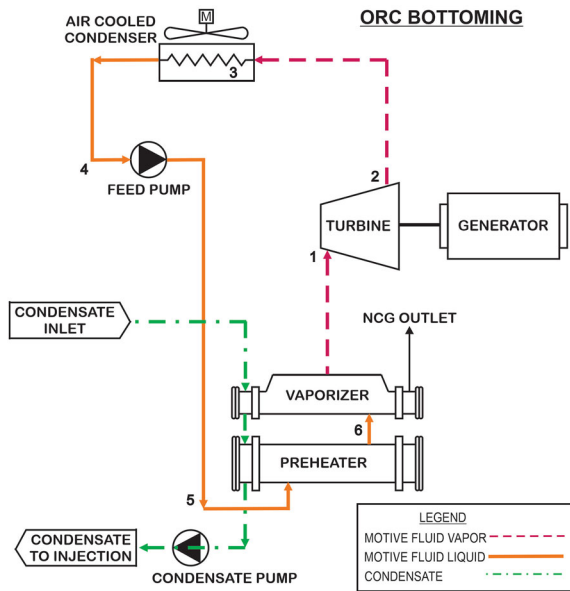**Figure 5.** Simplified process flow diagram for IGCCU.

Figure 6. Simplified process flow diagram for ORC Bottoming sub-unit. The numbers represent the thermodynamic state of the fluid in the pressure-enthalpy and temperature–entropy diagrams.

could be used to prevent solid deposition in a vaporizer, such as installing an additional solid basket or modifying the solid trap (Candido and Zarrouk 2017).

Thermodynamic process diagram for ORC Bottoming (DiPippo 2012, 2015a) is given in Figure 7. Mathematical expression of the thermodynamic processes is described as follows:

ORC Bottoming:

$$w_t = h_1 - h_2 \tag{7}$$

$$w_p = h_5 - h_4 \tag{8}$$

$$h_2 = h_1 - \eta_s(h_1 - h_{2s}) \tag{9}$$

$$\dot{m}_f = \frac{\dot{Q}_{in}}{(h_1 - h_5)} \tag{10}$$

$$\dot{W}_t = \dot{m}_f w_t \tag{11}$$

$$\dot{W}_p = \dot{m}_f w_p \tag{12}$$

$$\dot{W}_{ORC} = \dot{W}_t - \dot{W}_{parasitic} \tag{13}$$

$$\dot{W}_{parasitic} = \dot{W}_p + \dot{W}_c \tag{14}$$

In general, the thermodynamic process of the ORC Brine cycle using a recuperator (Fig. 8) is almost the same as the basic ORC Bottoming. The addition of a recuperator is equivalent to the addition of two points (2r and 5r) on the P–h and T–s diagrams (Fig. 9). The installation of a recuperator will increase
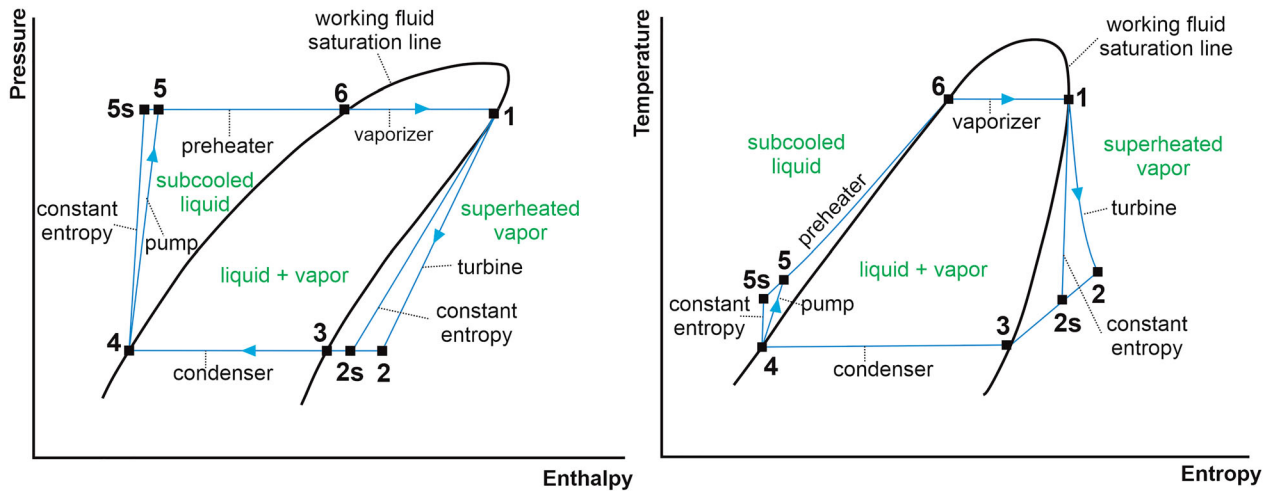
Figure 7. Pressure-enthalpy and temperature–entropy diagrams for ORC Bottoming. The numbers represent the thermodynamic state of fluid on the equipment for the ORC Bottoming subunit in the process flow diagram (Fig. 6).
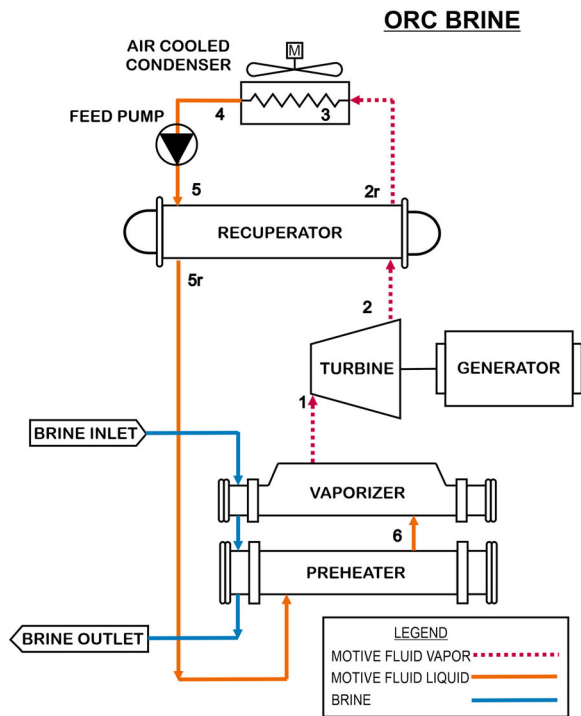

Figure 8. Simplified process flow diagram for ORC Brine subunit with recuperator. The numbers represent the thermodynamic state of the fluid in the pressure-enthalpy and temperature–entropy diagrams.

the thermal efficiency and reduces the amount of heat extracted from brine at the preheater. The equation to calculate the flow rate of working fluid in the ORC Brine cycle with a recuperator is:

$$\dot{m}_\mathrm{f} = \frac{\dot{Q}_\mathrm{in}}{(h_1 - h_{5r})} \qquad (15)$$

where $h_1, h_2, h_{2s}, h_4, h_5, h_{5r}$ are enthalpy of the fluid at different states (kJ/kg); $\dot{m}_\mathrm{f}$ is working fluid mass flow rate (kg/s); w_t is turbine specific energy (kJ/kg); $\dot{W}_\mathrm{t}$ is turbine power consumption (kJ/s or kW); w_p is pump specific energy (kJ/kg); $\dot{W}_\mathrm{p}$ is pump power consumption (kJ/s or kW); $\dot{W}_\mathrm{ORC}$ is power generated by ORC unit (kJ/s or kW); $\dot{W}_\mathrm{parasitic}$ is parasitic load (kJ/s or kW); $\dot{W}_\mathrm{c}$ is condenser power consumption (kJ/s or kW); η_s is turbine non-isentropic efficiency; and $\dot{Q}_\mathrm{in}$ is total heat supplied to the ORC cycle through evaporator and preheater (kJ/kg steam).

The parasitic load in IGCCU was mostly due to pump and condenser's fan load. The value of this load can be estimated based on a study by Mwagomba (2016). From this study, the parasitic load for condenser's fan is estimated to be around 12.37% of the gross power produced. Pump load can be calculated using simple thermodynamic calculation and assuming a 60% pump efficiency.

One of the critical parameters in designing an ORC system is the pinch point temperature difference (T_{pp}). A small T_{pp} value will result in an effective heat transfer process but will require a large heat transfer area that will have an impact on the economic value (Zeyghami 2015). In this re-
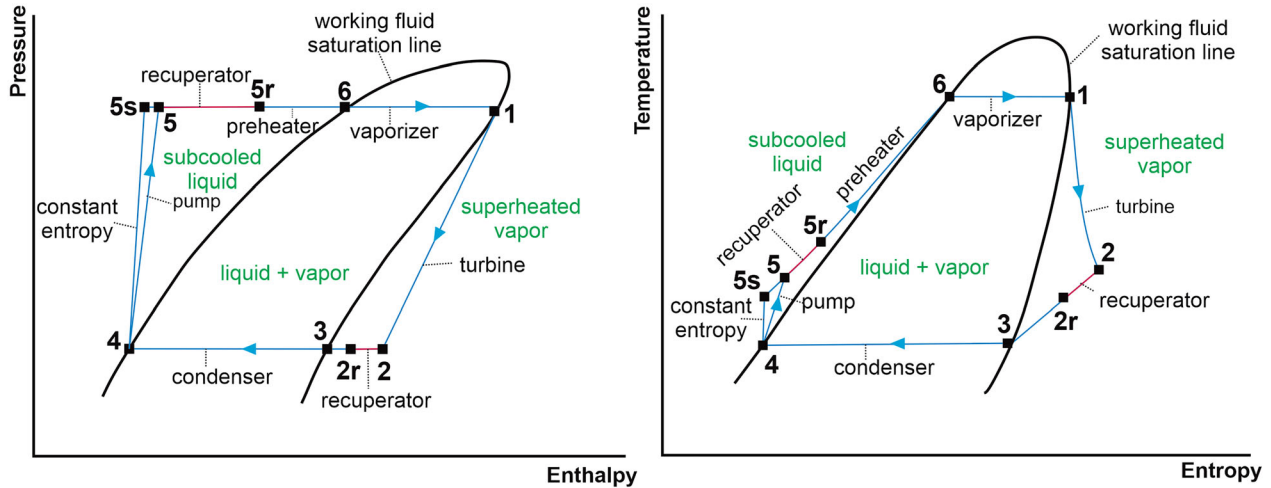
Figure 9. Pressure–enthalpy and temperature–entropy diagrams for ORC Brine subunit with recuperator. The numbers represent the thermodynamic state of fluid on the equipment for the ORC Brine sub-unit in the process flow diagram (Fig. 8).

search, the T_{pp} for ORC Brine and ORC Bottoming are 15.15 °C and 8.95 °C, respectively.

INTEGRATED RESULTS FOR 55 MW AND 2 × 55 MW POWER GENERATION SCENARIO

For this scenario, all existing wells were set to produce geothermal fluid until the power output decreases to 55 MW. When the power output decreases, then new make-up well is allowed to open. The production simulation then continues onward until the power output decreases again from 55 MW, in which case, more new make-up wells are open. This loop continues until the simulation reaches the year 2044 (30 years of production). The production simulation starts in the year 2016 with eight existing wells (Table 3).

There are two scenarios studied in this paper to generate electricity of 110 MW from a two-unit power plant. The first scenario is added another 55 MW DSCU, and this option will limit the geothermal fluid production only from the steam on the vapor-dominated zone. The second scenario is to add one unit of IGCCU generating 55 MW, and this unit will grant access to exploit the deep liquid reservoir.

Table 3. List of existing production wells

No	Well	Area
1	PPL-01	D
2	PPL-02	A
3	PPL-02A	A
4	PPL-03	B
5	PPL-03A	B
6	PPL-03B	B
7	PPL-05	B
8	PPL-07	C

Utilization of 1 × 55 MW DSCU (Scenario-1)

Figure 10 shows the steam production rate profile when 1 × 55 MW DSCU is utilized. The production rate ranges from 130 to 115 kg/s. 115 kg/s is the minimum steam production rate to maintain 55 MW capacity. The number of injection wells used in this scenario is 1 well, PPL-01B, which is the existing injection well. The injection rate at PPL-01B wells is 27 kg/s, with the enthalpy of water 104 kJ/kg (the enthalpy of water at a pressure of 1 atm and ambient temperature). The sudden increase in production rate shows a newly opened make-up well. The total make-up well needed for this scenario is six make-up wells.
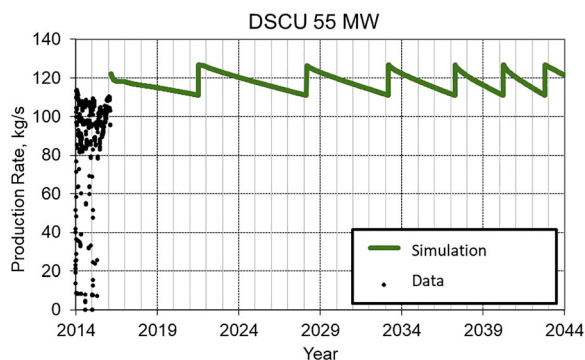
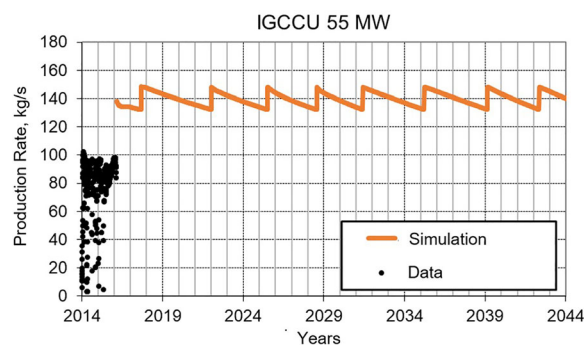**Figure 10.** Steam production rate using DSCU to maintain 55 MW power output.

Figure 11. Steam production rate using IGCCU to maintain 55 MW power output.

Utilization of 1 × 55 MW IGCCU (Scenario-2)

The production strategy of the 1 × 55 MW IGCCU is similar to 1 × 55 MW DCSU but it utilized only the STG and ORC Bottoming. This scenario is used to compare how the reservoir would perform and how much make-up wells needed if we utilize IGCCU instead of the existing DSCU. Figure 11 shows the steam production rate profile when 1 × 55 MW IGCCU is utilized. The electricity generation ranges between 55.0 and 61.5 MW or equivalent to 132–149 kg/s. For this scenario, two make-up wells are directly needed at the beginning of the simulation to maintain 55 MW minimum power output. In total, there are ten make-up wells needed to maintain 55 MW minimum capacity until the year 2044 and two reinjection wells (PPL-01A and PPL-01B). The injection rate at each well is 60 kg/s, and injection temperature to be the same as the temperature of the fluid exiting the ORC Bottoming Unit, which is 80 °C (335 kJ/kg).

Utilization of 2 × 55 MW DSCU (Scenario-3)

In this scenario, it is assumed that the power plant had been operated with one unit of DSCU from 2014 until 2019. The injection strategy is similar to 1 × 55 MW (Scenario-1) but with an almost double injection rate, in PPL-01A and PPL-01B. From the year 2014 to 2019, no make-up well is added. It is to simulate the model as close as possible to the actual field operation. In the year 2019, one more DSCU with the same 55 MW generation capacity is added; therefore, the total power generation capacity is 110 MW. In order to feed the sec-

Table 4. List of additional wells for 2 × 55 MW DSCU scenario

No	Well	Area
1	PPL-08A	A
2	PPL-14A	A
3	PPL-14B	A
4	PPL-14C	A
5	PPL-04B	A
6	PPL-02B	A
7	PPL-09A	C

ond DSCU with enough steam to generate 55 MW of electricity, seven new wells (Table 4) are added with a range of productivity index (PI) between 3.1E−12 and 5.9E−12 m^3 for TOUGH2 well on deliverability (Pruess et al. 1999).

The steam production profile to maintain 110 MW generating capacity from 2019 to 2044 is shown in Figs. 12 and 13. The production of steam ranges from 222 to 237 kg/s, which is equivalent to electricity production 110–118 MW. The 23 make-up wells are needed to maintain 110 MW generating capacity until 2044, and the time range between two make-up wells are getting closer. These are due to the relatively fast pressure decline in the steam zone.

Utilization of 1 × 55 MW DSCU and 1 × 55 MW IGCCU (Scenario-4)

In this scenario, IGCCU is used as the second power plant instead of DSCU. The new wells that feed IGCCU are not only from the steam zone but also from the brine reservoir. Therefore, the geothermal fluid produced is a mixture of steam and
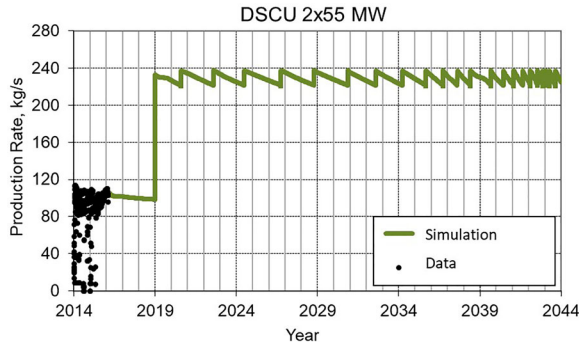
Figure 12. Steam production rate using 2×55 MW DSCU to maintain 110 MW power output.
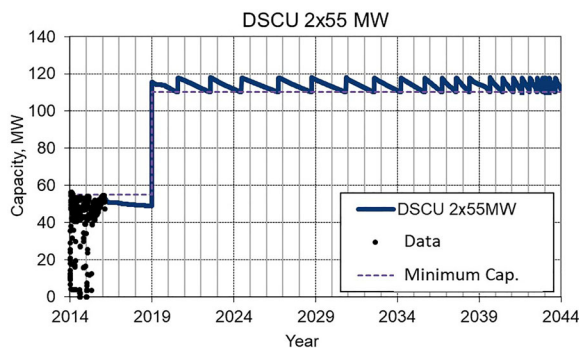

Figure 13. Power output profile using 2×55 MW DSCU to maintain 110 MW power output.

Table 5. List of additional wells for scenarios 1×55 MW DSCU and 1×55 MW IGCCU

No	Well	Area
1	PPL-14A	A
2	PPL-14B	A
3	PPL-14C	A
4	PPL-17	A
5	PPL-17A	A
6	PPL-17B	A
7	PPL-13	B
8	PPL-13A	B
9	PPL-13B	B
10	PPL-13C	B
11	PPL-11	B
12	PPL-11A	B
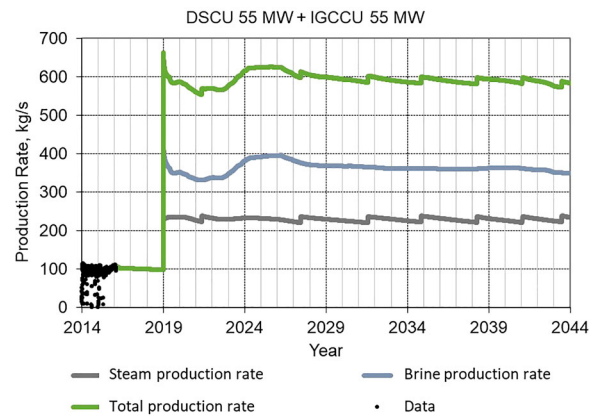
Figure 14. Steam and brine production rate for Scenario-4.

brine. The brine will be separated from steam and fed to the ORC Brine sub-unit of IGCCU, while the steam is then supplied to the STG and goes through in the ORC Bottoming sub-unit.

In the Scenario-4, additional wells that supply geothermal fluid to IGCCU in the model use a productivity index (PI) 5.0E−13–1.8E−12 m³ (Table 5). All these wells are produced from the deep liquid reservoir. The production wells from the water zone have different production rates. This is because the PI value is adjusted to the ability of the reservoir rock around the well to flow the fluid. If the PI is set too high, then the well will experience a very sharp decline in production, so the value of the PI is considered not to represent the ability of the reservoir to drain geofluid.

The injection wells needed in this scenario are five wells. There are already two existing injection wells (shallow injection) and three deep injection wells, which are PPL-12 (Area B), PPL-16A (Area-A), PPL-17C (Area-A). The maximum injection

rate for three new deep injection wells is limited to 150 kg/s. The injection wells are selected based on their distance from the production well to provide pressure support on the reservoir and avoid thermal breakthrough.

The make-up wells, on the other hand, are only produced from the steam zone. The results in Figure 14 show the production rate of both brine and steam. One exciting feature of these results is that the brine production rate is declining in the first 3 years of operation. After 3 years of operation, the production of brine increases to a certain level of production rate then declines with a relatively small decline rate compared to steam production decline. The rise of the brine production rate after 3 years of operation is due to the injection fluid from three deep injection wells and increased the feed zone pressure temporarily. There are seven make-up

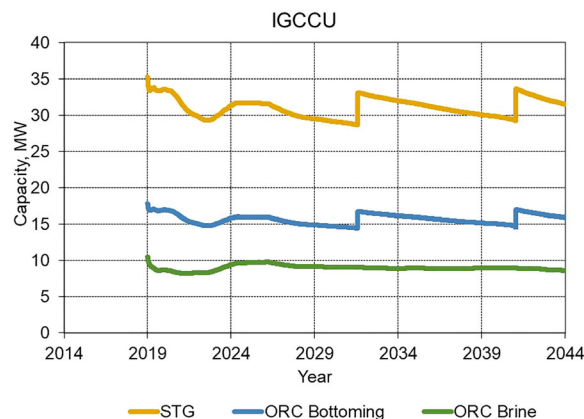**Table 6.** List of make-up wells for scenarios 1×55 MW DSCU and 1×55 MW IGCCU

No	Well	Area	Production Year	Unit
1	PPL-02B	A	4.5	DSCU
2	PPL-09A	C	10.6	DSCU
3	PPL-09B	C	14.7	IGCCU
4	PPL-09C	C	17.9	DSCU
5	PPL-09D	C	21.4	DSCU
6	PPL-07A	C	24.2	IGCCU
7	PPL-07B	C	26.6	DSCU

Figure 15. IGCCU Unit in additional 1×55 MW.

Figure 16. Power generation profile for Scenario-4.

wells needed for this scenario with a range of PI $3.9E{-}13$–$9.2E{-}12$ m^3 (Table 6). The total new wells (additional wells plus make-up wells) required in this scenario are 19.
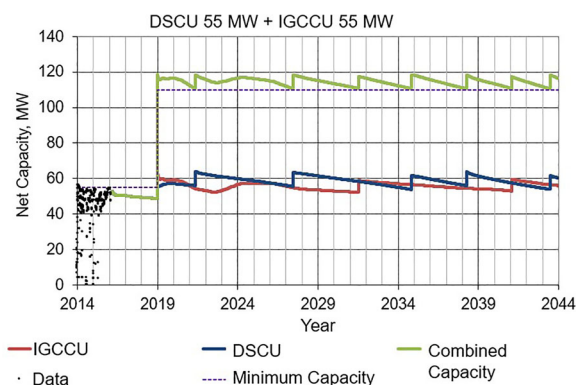
The simulation shows the total geothermal fluid produced ranges from 560 to 670 kg/s, with steam and brine production rates ranging from 210 to 230 kg/s and 330 to 395 kg/s (Fig. 14). For brine production, all brines are channeled to IGCCU (ORC Brine sub-unit). The second Unit (IGCCU 1×55 MW) electricity distribution from sub-unit was utilized a sub-unit STG, ORC Bottoming, and ORC Brine shown in Figure 15. All make-up wells are produced from the vapor zone, both for DSCU and IGCCU. In this scenario, the make-up well was opened when the total capacity produced was less than 110 MW. Even though one of the units is produced under 55 MW, the make-up well will not be opened if the total capacity is still above 110 MW. The steam produced from the make-up well has only flowed to the operating units with the lowest electricity capacity. For example, if the total capacity is below 110 MW, the make-up well is opened. If, at that time, the production capacity of DSCU were lower than that of the IGCCU, steam would be channeled to DSCU. The total capacity produced by the two units is shown in Figure 16. The total electricity capacity produced ranges from 119 to 110 MW.

Production, Injection, and Make-up Well

In the 55 MW generation scenario using DSCU when the production zone is from the steam zone only, the use of DSCU requires fewer make-up wells, specifically seven wells, while the IGCCU requires ten make-up wells in deep liquid reservoir. In the 55 MW generation scenario, the use of DSCU is considered to have a better impact on the aspects of sustainable production than the use of IGCCU because the use of DSCU provides a smaller reduction of pressures and temperatures in all reservoir areas.

The summary of production, injection, and make-up wells for each scenario is shown in Figure 17. In the 110 MW (2×55 MW) generation scenario, the use of the DSCU provides a higher number of make-up wells than the use of the IGCCU, where the DSCU requires 30 make-up wells, while IGCCU produced from the steam and water zones needs only eight make-up wells. Nevertheless, the second DSCU only requires only seven additional production wells, while the IGCCU requires 12 additional production wells plus three new injection wells. In the 2×55 MW generation scenario, the use of the DSCU as the second unit gives a more significant pressure and temperature reduction than the IGCCU. Thus, it can be concluded that
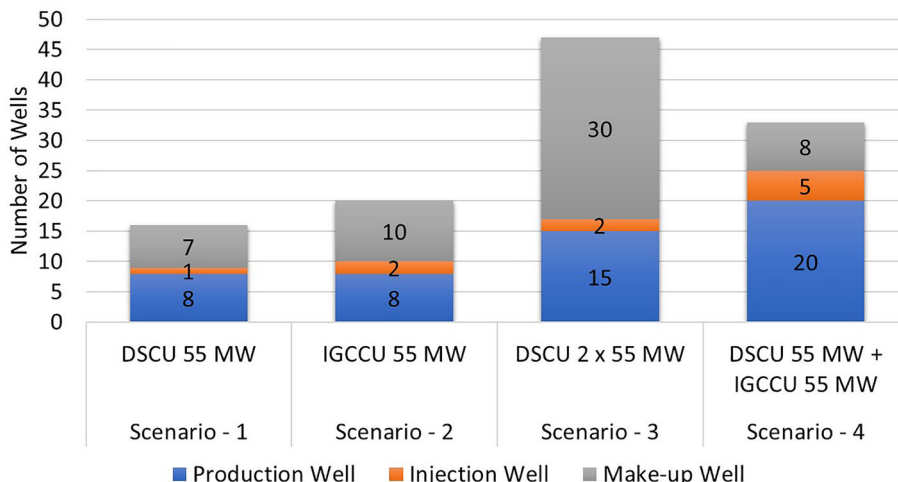
Figure 17. Summary of production, injection, and make-up wells for each scenario.

the use of the IGCCU for Unit-2 has a better impact on the aspects of sustainable production.

RESULTS

The IGCCU requires not only more make-up wells but also more steam flow rate to maintain minimum power output until the year 2044 (28 years operation starting from simulation time). It is due to IGCCU being less efficient than DSCU with SGC value of 2.016 kg/s/MW. IGCCU has an SGC value of 2.562 kg/s/MW, 6.5 kg/s/MW, and 40.4 kg/s/MW for the Steam Turbine Generator units, ORC Bottoming units, ORC Brine units, respectively. The changes of reservoir characteristic in the steam zone were monitored by measurement of subsurface pressures, temperatures, gas saturation (SG) (Fig. 18). It was represented by blocks at 700 masl, while the changes and forecast of fluid properties in the reservoir are shown in Figures 19, 20, 21, 22, 23 ,and 24.

The change and forecast of pressure profiles in the steam zone are shown in Figs. 19 and 20. The pressure decline along the steam zone is higher and broader when IGCCU is utilized for 55 MW. It is because IGCCU needs a higher steam flow rate to produce the same power output than DSCU. Higher steam consumption leads to accelerated pressure decline. From these results, we can conclude that DSCU gives better sustainability than IGCCU. It is valid for 55 MW power generation and when the
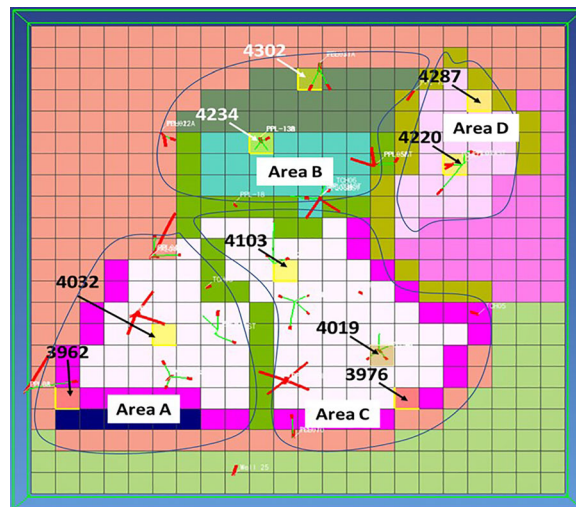

Figure 18. Location and block number for monitoring: Area A-4032, Area B-4234, Area C-4103, and Area D-4287. The colors of each grid block represent the material properties given in Table 2.

only steam zone is exploited. The DSCU 2 × 55 MW has a higher pressure decline among all scenarios. Nevertheless, DSCU 55 MW plus IGCCU 55 MW had a relatively stable pressure decline because the production in the brine for IGCCU gives pressure support to the steam zone because of boiling in the transition zone to produce steam from a deep liquid reservoir.

The IGCCU provides a higher temperature drop for 55 MW, especially in blocks near the production wells (Fig. 21). In contrast, the 2 × 55 MW

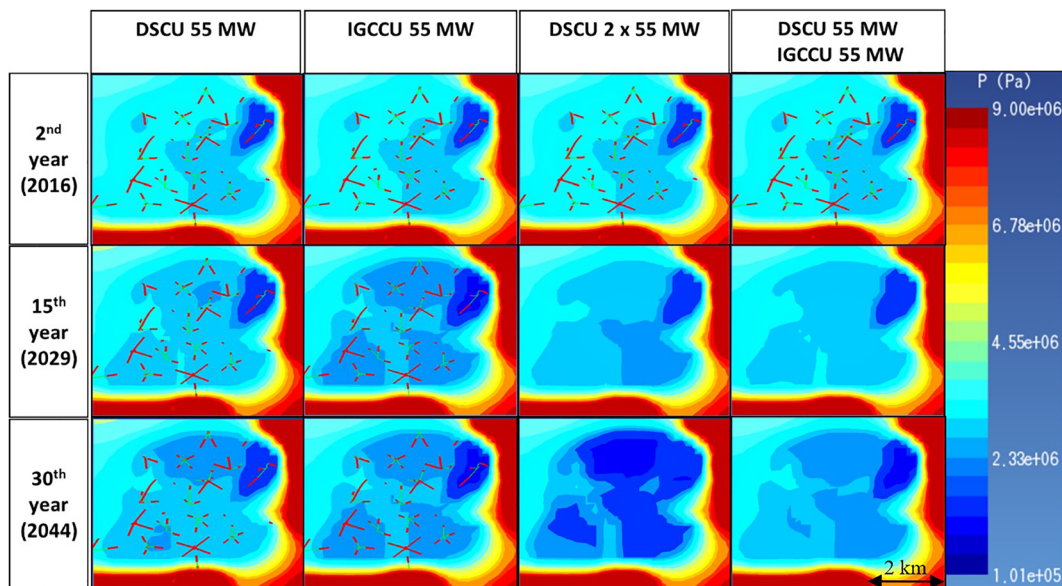**Figure 19.** Changes in reservoir pressure profile at 700 masl (steam zone) for each scenario.
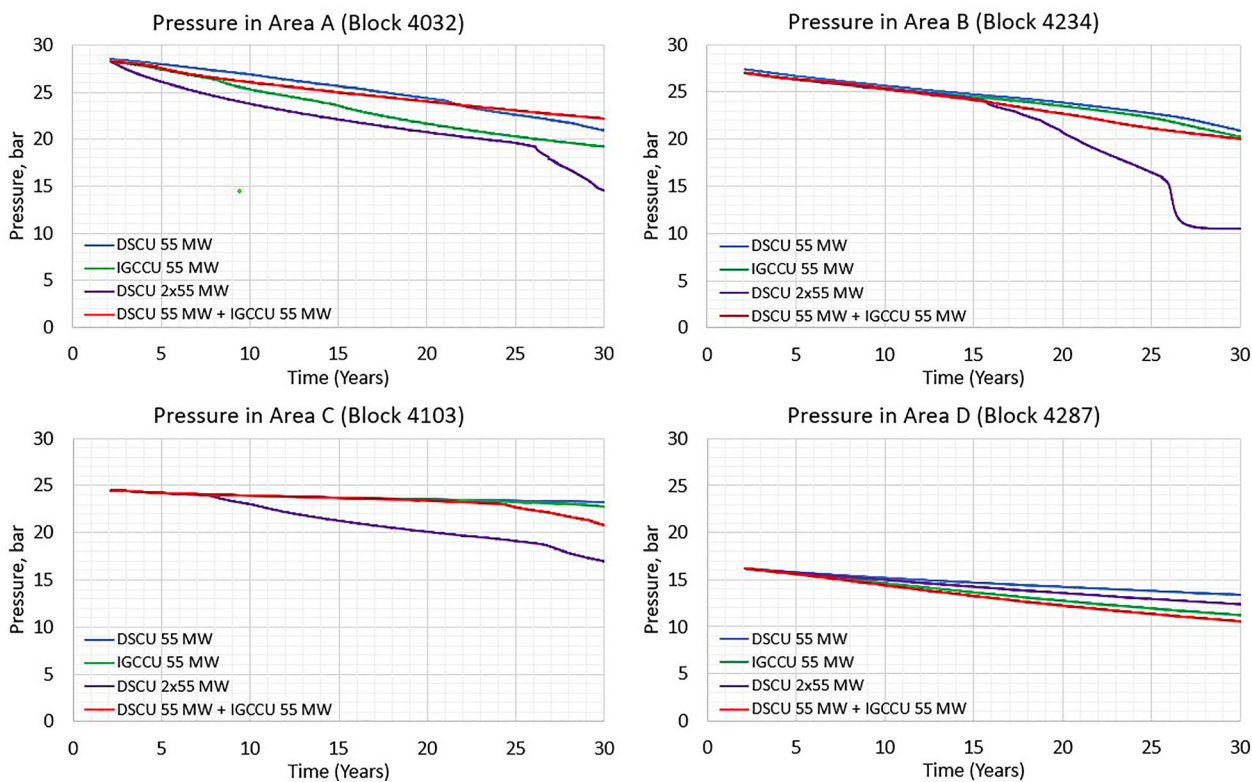

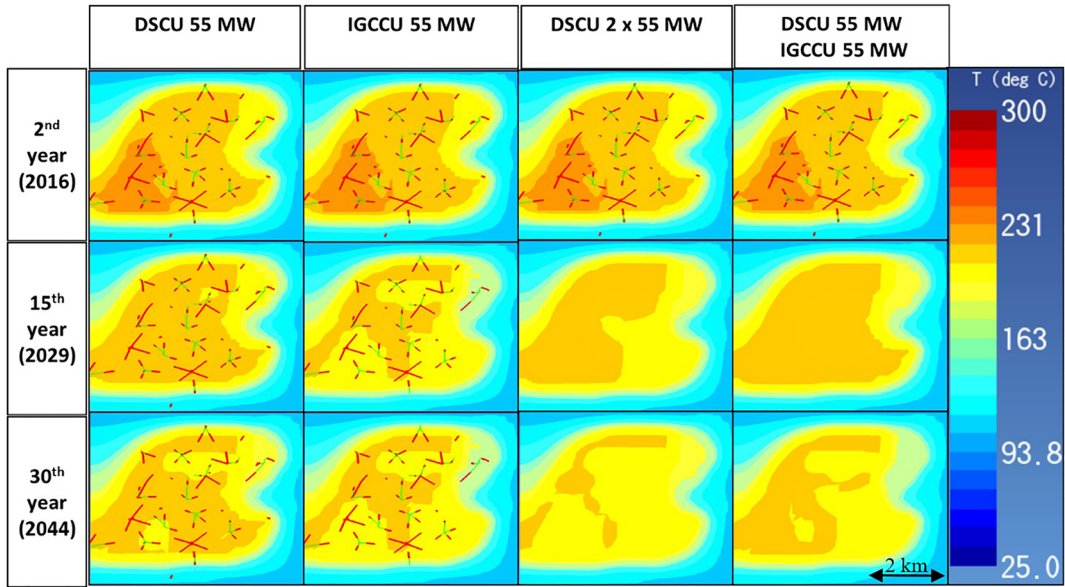**Figure 20.** Pressure forecast for all scenarios.

Figure 21. Changes in reservoir temperature profile at 700 masl (steam zone) for each scenario.
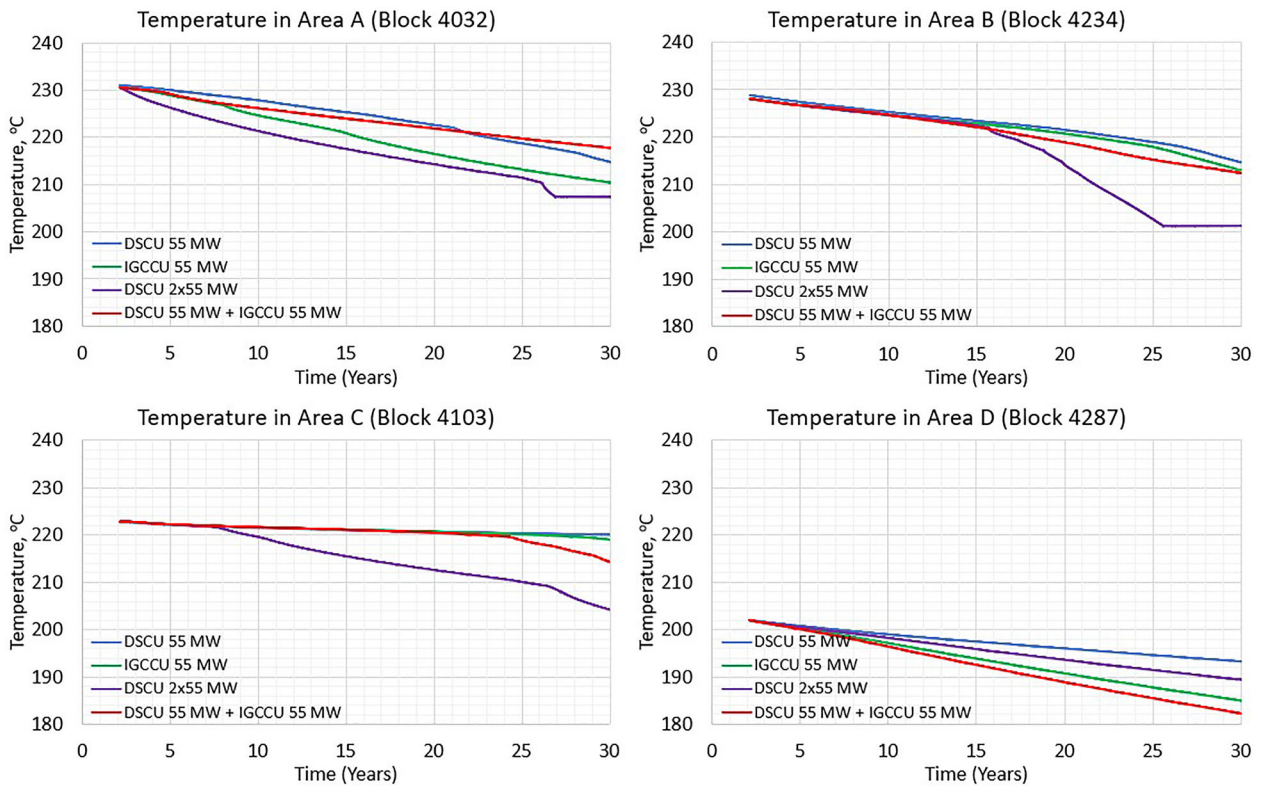

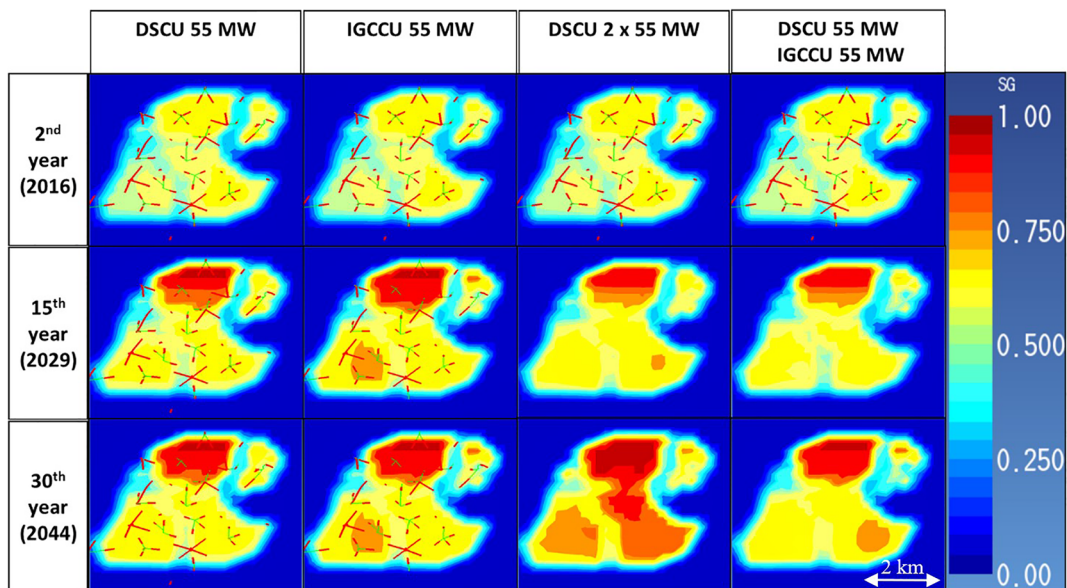**Figure 22.** Temperature forecast for all scenarios.

Figure 23. Changes in gas saturation (SG) profile at 700 masl (steam zone) for each scenario.
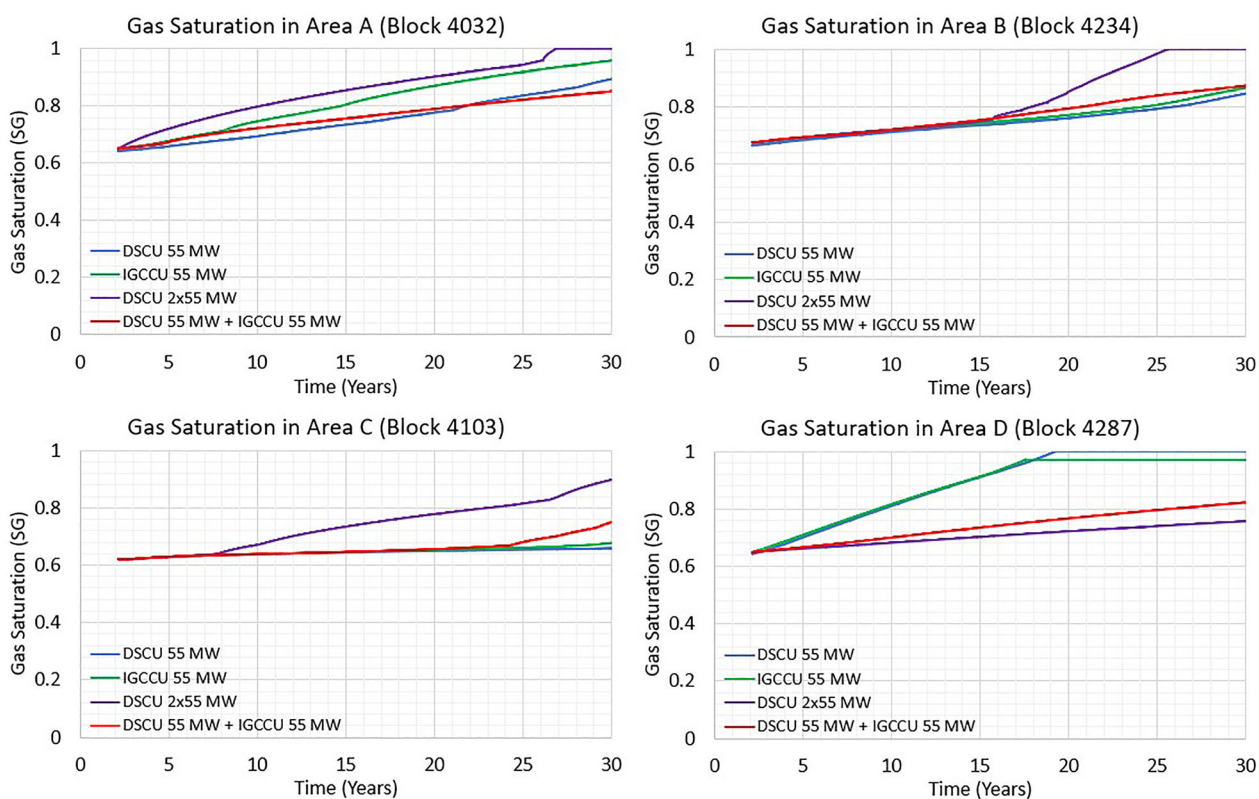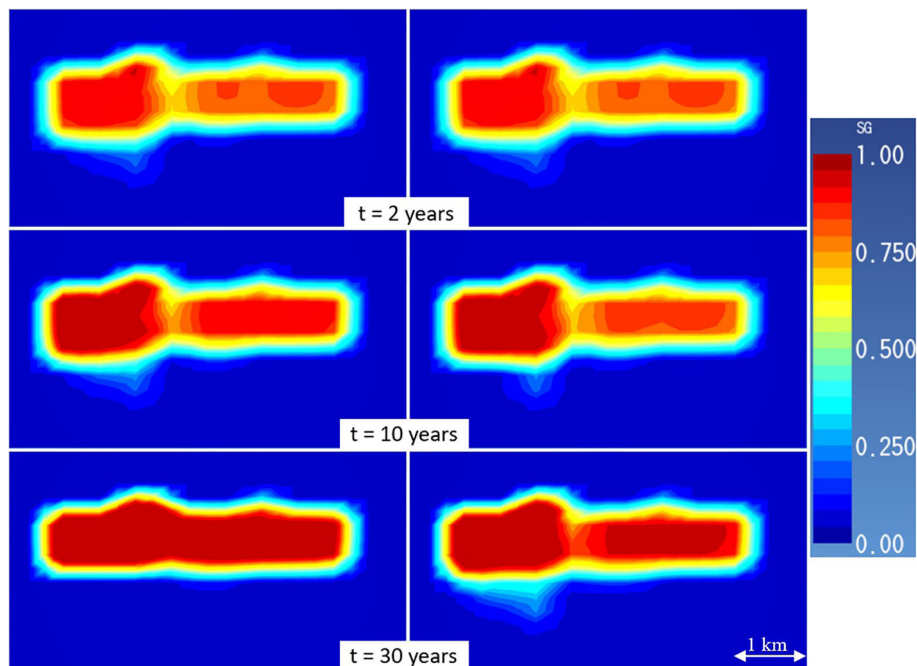

Figure 24. Gas saturation (SG) forecast for all scenarios.

Figure 25. Gas saturation (SG) changes in reservoir sections (cross section in the middle at $x = 3000$) at different times for the scenarios DSCU 2 × 55 MW (left) and DSCU 55 MW + IGCCU 55 MW (right).

of DSCU had a wider cooling effect spread over steam zone. Blocks that are farther from the production wells generally do not experience a temperature difference as big as the blocks that are close to the production wells (Fig. 22).

The changes in gas saturation during production for each scenario are shown in Figures 23 and 24. Gas saturation generally increases during production. The gas saturation in IGCCU tends to be higher than DSCU for 55 MW. These are caused by a higher pressure drop on IGCCU so that the reservoir fluid experiences a more intensive flashing process. Significant increases in gas saturation were also observed in the steam zone for 2 × 55 MW DSCU; this is also due to the opening of the 30 make-up wells. This process leads to a superheated zone in the reservoir.

The gas saturation value in the vapor zone is getting bigger, especially in the exploited area. Besides, it appears that the boiling zone is also thickened in both scenarios. The thickening of the boiling zone takes place throughout the steam production process. However, in the 2 × 55 MW DSCU scenario, the thickening stops at a certain point and turns into depletion of the boiling zone. Until the year of 30th (Fig. 25), the boiling zone that was

thickened disappears. The reason is that production from the vapor zone reduces reservoir pressure so that the water level rises. At the beginning of the production, the pressure difference between the steam zone and the hydrostatic pressure of the water is not too significant; hence, the rate of evaporation is still faster than the rate of increase in the water level. In this condition, the evaporation process is more dominant so that the boiling zone thickens. As steam production progresses, the pressure in the vapor zone decreases, and the pressure difference between the vapor zone and the hydrostatic pressure increases to the point that the rate of water level rise is faster than the rate of evaporation. In this condition, the boiling zone is running low because the water level is rising. This phenomenon only happens in the 2 × 55 MW DSCU scenario but does not occur in the 55 MW DSCU + IGCCU 55 MW scenario.

DISCUSSION

The IGCCU causes more significant pressure and temperature decline than the DSCU. In addition, to maintain the capacity of 55 MW, IGCCU

needs more make-up wells. The use of DSCU is more suitable than IGCCU if the production only comes from the steam zone. DSCU electricity generation is more efficient than IGCCU, which is indicated by a lower SSC value. The impact is that the mass taken from the reservoir is not as much as when using IGCCU.

The utilization of DSCU 110 MW causes faster expansion of low pressure and low temperature zones. An intensive increase in gas saturation occurring in the DSCU scenario is due to a higher pressure drop. For the development of Unit-II power plant, it is recommended to continue using DSCU (the same as Unit-I) if production only comes from the steam zone, but it is better to use IGCCU for Unit-II if brine can be produced from the deep liquid reservoir. The production would be more optimal because IGCCU has an ORC Brine sub-unit that can extract energy from the brine.

The DSCU utilization to produce 110 MW net power output for 30 years still be possible but requires far more make-up wells and causes higher pressure and temperature decline in the steam zone. A combination of DSCU and IGCCU gives better sustainability to the reservoir. This is exposed by lesser pressure drops in the steam zone. The combination of DSCU and IGCCU also requires fewer make-up wells. Although it requires more production wells in the beginning, the total well required is still less. These results also happened in the previous study done by Pratama and Saptadji (2016, 2018) for a generic geothermal reservoir.

Deeper exploitation of the brine zone certainly increases drilling costs and surges the investment cost of IGCCU technology, which consists of many subunits. Thus, the investment expenses of additional wells produced from the deep liquid reservoir need to be determined at an early stage of development. In the case of the Patuha geothermal field, although it is not at the initial stage development, the liquid reservoir must be studied intensively in order to provide certainty of a suitable production well location. The production from the brine zone requires an integrated production-injection scenario as it is possible that the exact location of the injection well is at a high elevation.

The IGCCU yields better sustainability than adding one more DSCU to generate 110 MW electricity, and technical feasibility aspects still need to be evaluated since exploiting the liquid reservoir requires deeper drilling. The exploitation of the deep liquid reservoir requires more intensive re-search to understand the zone, and thus, to increase the success ratio. The complexity of the IGCCU might also add more capital expenses if this unit is to be used. Therefore, a financial feasibility study needs to be conducted to complement its technical feasibility. Based on the latest research, Lesmana et al. (2020) and Winofa et al. (2020) state that the results of the numerical reservoir model is very fit to be used as an input parameter from a technical aspect to increase the level of confidence in the financial model. Their study uses a probabilistic financial model to reduce high uncertainty input parameters.

CONCLUSIONS

The 55 MW, power generation scenario, using the Dry-steam Cycle Unit (DSCU) to extract energy from the steam zone only is a preferable option than using the Integrated Geothermal Combined-Cycle Unit (IGCCU). This option will yield better sustainability, which is indicated by less make-up well required and less steam consumption for each megawatt of power generated. The 110 MW, power generation scenario, using two DSCU generating 55 MW each is not the optimal option since it can only be produced from the steam zone; therefore, this accelerates the depletion rate of the steam zone. Adding one 55 MW IGCCU to the existing 55 MW DSCU is a more optimal option since the IGCCU opens the possibility to extract energy from the deep liquid reservoir. This option, in turn, will act as a buffer to maintain the depletion rate of the steam zone at a minimum level.

The future work of this research is to update the conceptual model based on the latest data. The updated conceptual model is needed to revise the reservoir numerical model. Therefore, an assessment of probabilistic resources can be carried out using Experimental Design (ED) and Surface Response Methods (RSM) to include uncertainty parameters. This method can also be used to calculate the probability of discovery (PoD) production capacity for the development of wells and make-up wells. The next research is to combine the results of numerical models that have captured uncertainty from a reservoir, production, power plant, and development to be used in probabilistic financial models to get a high level of confidence from the results of the feasibility study.

ACKNOWLEDGMENT

REFERENCES

Alamsyah, O., Bratakusuma, B., Hoang, V., & Roberts, J. W. (2005). Dynamic modeling of Darajat field using numerical simulation. In *Proceedings world geothermal congress*, (April) (pp. 24–29).

Ashat, A., & Pratama, H. B. (2018). Application of experimental design in geothermal resources assessment of Ciwidey-Patuha, West Java, Indonesia. In *IOP conference series: Earth and environmental science*, (Vol. 103(1)). https://doi.org/10.1088/1755-1315/103/1/012009.

Ashat, A., Pratama, H. B., & Itoi, R. (2019a). Updating conceptual model of Ciwidey-Patuha geothermal using dynamic numerical model. In *IOP conference series: Earth and environmental science*, (Vol. 254(1)) . https://doi.org/10.1088/1755-1315/254/1/012010.

Ashat, A., Pratama, H. B., & Itoi, R. (2019b). Comparison of resource assessment methods with numerical reservoir model between heat stored and experimental design: Case study Ciwidey-Patuha geothermal field. In *IOP conference series: Earth and environmental science*, (Vol. 254(1)). https://doi.org/10.1088/1755-1315/254/1/012011.

Bixley, P. F., Clotworthy, A. W., & Mannington, W. I. (2009). Evolution of the Wairakei geothermal reservoir during 50 years of production. *Geothermics, 38*(1), 145–154.

Bogie, I., Kusumah, Y. I., & Wisnandary, M. C. (2008). Overview of the Wayang Windu geothermal field, West Java. *Indonesia. Geothermics, 37*(3), 347–365.

Candido, C. A. S., & Zarrouk, S. J. (2017). Scaling mitigations for the binary plant vaporizer: Upper Mahiao, the scaling mitigations for the binary plant vaporizer: Upper Mahiao, the Philippines. In *Proceedings 39th New Zealand Geothermal Workshop*, 1(November).

DiPippo, R. (2012). *Geothermal power plants: Principles, applications, case studies and environmental impact* (3rd ed.). Butterworth-Heinemann: Oxford. https://doi.org/10.1016/C2014-0-02885-7.

DiPippo, R. (2015a). *Geothermal power plants: Principles, applications, case studies and environmental impact* (4th ed.). Butterworth-Heinemann: Oxford. https://doi.org/10.1016/B978-0-08-087872-0.00708-3.

DiPippo, R. (2015b). Geothermal power plants: Evolution and performance assessments. *Geothermics, 53,* 291–307. https://doi.org/10.1016/j.geothermics.2014.07.005.

Elfina. (2017). Updated conceptual model of the Patuha Geothermal Field, Indonesia. *UNU-GTP*, (10), 89–112. https://orkustofnun.is/gogn/unu-gtp-report/UNU-GTP-2017-10.pdf.

Franco, A., & Vaccaro, M. (2012). An integrated "Reservoir-Plant" strategy for a sustainable and efficient use of geothermal resources. *Energy, 37*(1), 299–310.

Hamdani, M. R., Pratama, H. B., & Sutopo, (2020). Updating the Conceptual Model of Lumut Balai Geothermal Field, South Sumatera, Indonesia Using Numerical Simulation. In *IOP conference series: Earth and environmental science*, (Vol. 417(1)). https://doi.org/10.1088/1755-1315/417/1/012023.

Hoang, V., Alamsyah, O., & Roberts, J. (2005). Darajat geothermal field expansion performance—A probabilistic forecast. In *Proceedings World Geothermal Congress 2005*.

Intani, R. G., Golla, G. U., Syaffitri, Y., Paramitasari, H. M., Nordquist, G. A., Nelson, C., et al. (2020). Improving the conceptual understanding of the Darajat Geothermal Field. *Geothermics, 83,* 101716.

Kaya, E., Zarrouk, S. J., & O'Sullivan, M. J. (2011). Reinjection in geothermal fields: A review of worldwide experience. *Renewable and Sustainable Energy Reviews, 15*(1), 47–68.

Kaypakoglu, B., & Barbon, U. (2019). An evaluation of single flash power plants with ORC bottoming units at high NCG content. In *Proceedings 44th workshop on geothermal reservoir engineering, 1* (pp. 1–7).

Koestono, H., Siahaan, E. E., Silaban, M., & Franzson, H. (2010). Geothermal model of the Lahendong geothermal field, Indonesia. In *Proceedings world geothermal congress*, (April), (pp. 25–29).

Layman, E., & Soemarinda, S. (2003). The Patuha vapor-dominated resource West Java, Indonesia. In *The 28th Workshop on Geothermal Reservoir Engineering Proceedings* (pp. 357–364). Amsterdam: Elsevier.

Lesmana, A., Pratama, H. B., Ashat, A., Saptadji, N. M., & Gunawan, F. (2019). An updated conceptual model of the Tompaso geothermal field using numerical simulation. In *Proceedings 41st New Zealand geothermal workshop*.

Lesmana, A., Winofa, N. C., Pratama, H. B., Ashat, A., & Saptadji, N. M. (2020). Preliminary financial modelling with probabilistic approach for geothermal development project in Indonesia. In *IOP conference series: Earth and environmental science*, (Vol. 417(1)). https://doi.org/10.1088/1755-1315/417/1/012024.

Mannington, W., O'Sullivan, M., & Bullivant, D. (2004). Computer modelling of the Wairakei–Tauhara geothermal system, New Zealand. *Geothermics, 33*(4), 401–419.

Monterrosa, M., & Montalvo López, F. E. (2010). Sustainability analysis of the Ahuachapán geothermal field: Management and modeling. *Geothermics, 39*(4), 370–381.

Mulyadi, & Ashat, A. (2011). Reservoir modeling of the Northern Vapor-dominated two-phase zone of the Wayang Windu Geothermal Field, Java, Indonesia. In *Proceedings of 36th Stanford Geothermal Workshop* (pp. 1–7).

Mwagomba, T. (2016). *Preliminary Technical and Economic Feasibility Study of Binary Power Plant for Chiweta Geothermal Field, Malawi*. *UNU-GTP* (Vol. 1).

Nemčok, M., Moore, J. N., Christensen, C., Allis, R., Powell, T., Murray, B., et al. (2007). Controls on the Karaha-Telaga Bodas geothermal reservoir, Indonesia. *Geothermics, 36*(1), 9–46.

Noorollahi, Y., & Itoi, R. (2011). Production capacity estimation by reservoir numerical simulation of northwest (NW) Sabalan geothermal field, Iran. *Energy, 36*(7), 4552–4569.

O'Sullivan, M. J., Yeh, A., & Mannington, W. I. (2009). A history of numerical modelling of the Wairakei geothermal field.

Geothermics, 38(1), 155–168. https://doi.org/10.1016/j.geothe rmics.2008.12.001.

Ozcan, N. Y., & Gokcen, G. (2013). Performance analysis of single-flash geothermal power plants: Gas removal systems point of view. *Geothermal Energy, Technology and Geology*, (April) (pp. 227–260).

Porras, E. A., Tanaka, T., Fujii, H., & Itoi, R. (2007). Numerical modeling of the Momotombo geothermal system, Nicaragua. *Geothermics, 36*(4), 304–329.

Prabata, W., Sutopo, S., & Pratama, H. B. (2019). Experimental design and response surface method application in resources assessment: Case study Karaha-Talaga bodas, West Java, Indonesia. In *IOP conference series: Earth and environmental science,* (Vol. 254(1)). https://doi.org/10.1088/1755-1315/254/ 1/012026.

Pratama, H. B., & Saptadji, N. M. (2016). Numerical simulation for natural state of two-phase liquid dominated geothermal reservoir with Steam Cap Underlying Brine Reservoir. In *IOP conference series: Earth and environmental science*. h ttps://doi.org/10.1088/1755-1315/42/1/012006.

Pratama, H. B., & Saptadji, N. M. (2018). Study of sustainable production in two-phase liquid dominated with steam cap underlying brine reservoir by numerical simulation. In *IOP conference series: Earth and environmental science* (Vol. 103). https://doi.org/10.1088/1755-1315/103/1/012005.

Pratama, H. B., Supijo, M. C., & Sutopo, (2020). Experimental design and response surface method in geothermal energy: A comprehensive study in probabilistic resource assessment. *Geothermics, 87,* 101869.

Pruess, K., Oldenburg, C., & Moridic, G. (1999). *TOUGH2 User's Guide Version 2.0. Report LBNL-43134, Lawrence Berkeley National Laboratory, California Lawrence Berkeley National Laboratory*. http://escholarship.org/uc/item/4df6700h.pdf%5 Cnhttp://esd1.lbl.gov/FILES/research/projects/tough/docume ntation/TOUGH2_V2.0_Users_Guide.pdf.

Quinao, J. J. D., & Zarrouk, S. J. (2018). Geothermal resource assessment using experimental design and response surface methods: The Ngatamariki geothermal field, New Zealand. *Renewable Energy, 116,* 324–334.

Raharjo, I. B., Allis, R. G., & Chapman, D. S. (2016). Volcano-hosted vapor-dominated geothermal systems in permeability space. *Geothermics, 62,* 22–32.

Rivera Diaz, A., Kaya, E., & Zarrouk, S. J. (2016). Reinjection in geothermal fields—A worldwide review update. *Renewable and Sustainable Energy Reviews, 53,* 105–162.

Romagnoli, P., Arias, A., Barelli, A., Cei, M., & Casini, M. (2010). An updated numerical model of the Larderello–Travale geothermal system, Italy. *Geothermics, 39*(4), 292–313.

Seyedrahimi-Niaraq, M., Doulati Ardejani, F., Noorollahi, Y., Porkhial, S., Itoi, R., & Jalili Nasrabadi, S. (2019). A three-dimensional numerical model to simulate Iranian NW Sabalan geothermal system. *Geothermics, 77,* 42–61.

Supijo, M. C., Pratama, H. B., & Sutopo. (2019). The application of experimental design using three-level full factorial design for probabilistic resource assessment in Atadei Geothermal Field, Indonesia 4 Publications 4 Citations See Profile. In *The 7th Indonesia international geothermal convention & exhibition (IIGCE) 2019 proceedings*. https://www.researchgate.net/ publication/337886855.

Supijo, M. C., Pratama, H. B., & Sutopo. (2020). Response surface method using Box–Behnken design for probabilistic resource assessment: A case study in Atadei geothermal field, Indonesia. In *IOP conference series: Earth and environmental science* (Vol. 417(1)). https://doi.org/10.1088/1755-1315/417/1/ 012022.

Supijo, M. C., Wahjono, A. D., Lesmana, A., Harahap, A. H., Sutopo, Pratama, H. B., & Prabata, T. W. (2018). Updating conceptual model using numerical modelling for geothermal green field prospect Area in Atadei, East Nusa Tenggara, Indonesia. In *The 6th Indonesia international geothermal convention & exhibition (IIGCE) 2018 proceedings*.

Suryadarma, Dwikorianto, T., Zuhro, A. A., & Yani, A. (2010). Sustainable development of the Kamojang geothermal field. *Geothermics, 39*(4), 391–399.

Sutopo, Prabata, W., & Pratama, H. B. (2019). *The development study of Karaha–Talaga Bodas geothermal field using numerical simulation*. Berlin: Springer. https://doi.org/10.118 6/s40517-019-0139-2.

Winofa, N. C., Lesmana, A., Pratama, H. B., Saptadji, N. M., & Ashat, A. (2020). The application of numerical simulation result for geothermal financial model with probabilistic approach: A comprehensive study. In *IOP conference series: Earth and environmental science*, (Vol. 417(1)) https://doi.or g/10.1088/1755-1315/417/1/012020.

Wolf, N., & Gabbay, A. (2015). Sarulla 330 MW geothermal project key success factors in development. *Transactions - Geothermal Resources Council, 39*(April), 907–912.

Yahara, T., & Tokita, H. (2010). Sustainability of the Hatchobaru geothermal field, Japan. *Geothermics, 39*(4), 382–390.

Zarrouk, S. J., & Moon, H. (2014). Efficiency of geothermal power plants: A Worldwide review. *Geothermics, 51,* 142–153.

Zeyghami, M. (2015). Performance analysis and binary working fluid selection of combined flash-binary geothermal cycle. *Energy, 88,* 765–774.